

An NMR and MD Study of Complexes of Bacteriophage Lambda Lysozyme with Tetra- and Hexa-N-acetylchitohexaose

Running title: Complexes of λ lysozyme and NAG polymers

Aysegul Turupcu,^[a] Alice M. Bowen,^[b] Alexandre Di Paolo,^[c,e] André Matagne,^[c] Chris Oostenbrink,^[a] Christina Redfield,^[d] and Lorna J. Smith^{*[b]}

[a] Institute of Molecular Modeling and Simulation, University of Natural Resources and Life Sciences Vienna, Vienna, Austria.

[b] Department of Chemistry, University of Oxford, Oxford, U.K.

[c] Laboratoire d'Enzymologie et Repliement des Protéines, Centre d'Ingénierie des Protéines, Institut de Chimie, Université de Liège, Belgium.

[d] Department of Biochemistry, University of Oxford, Oxford U.K.

[e] Current address: Kaneka Eurogentec S.A., Biologics, Liège Science Park, Rue Bois Saint jean 14, B-4102 Seraing, Belgium

Email address of corresponding author: lorna.smith@chem.ox.ac.uk

Key words: lysozymes, molecular dynamics, NMR spectroscopy, oligosaccharides, ligand binding

Abbreviations: Molecular dynamics (MD), Nuclear Magnetic Resonance (NMR), hexa-N-acetylchitohexaose (NAG6), tetra-N-acetylchitohexaose (NAG4), N-acetylmuramic acid (NAM), N-acetylglucosamine (NAG), Heteronuclear Single Quantum Correlation (HSQC), Protein Data Bank (PDB), lysozyme from T4 bacteriophage (T4L), Biological Magnetic Resonance Data Bank (BMRB), Simple Point Charge (SPC)

Abstract

The X-ray structure of lysozyme from bacteriophage lambda (λ lysozyme) in complex with the inhibitor hexa-N-acetylchitohexaose (NAG6) (PDB:3D3D) has been reported previously showing sugar units from two molecules of NAG6 bound in the active site. One NAG6 is bound with four sugar units in the ABCD sites and the other with two sugar units in the E'F' sites potentially representing the cleavage reaction products; each NAG6 cross links two neighbouring λ lysozyme molecules. Here we use NMR and MD simulations to study the interaction of λ lysozyme with the inhibitors NAG4 and NAG6 in solution. This allows us to study the interactions within the complex prior to cleavage of the polysaccharide. $^1\text{H}^{\text{N}}$ and ^{15}N chemical shifts of λ lysozyme resonances were followed during NAG4/NAG6 titrations. The chemical shift changes were similar in the two titrations, consistent with sugars binding to the cleft between the upper and lower domains; the NMR data show no evidence for simultaneous binding of a NAG6 to two λ lysozyme molecules. Six 150 ns MD simulations of λ lysozyme in complex with NAG4 or NAG6 were performed starting from different conformations. The simulations with both NAG4 and NAG6 show stable binding of sugars across the D/E active site providing low energy models for the enzyme-inhibitor complexes. The MD simulations identify different binding subsites for the 5th and 6th sugars consistent with the NMR data. The structural information gained from the NMR experiments and MD simulations have been used to model the enzyme-peptidoglycan complex.

Introduction

Lysozymes are very widespread throughout nature, being found in phage, bacteria, plants and animals.¹ Along with the lytic transglycosylases they are collectively known as N-acetyl- β -D-muramidases cleaving the β -1,4-glycosidic bond between N-acetylmuraminic acid (NAM) and N-acetylglucosamine (NAG) of the bacterial peptidoglycan.² The difference between these enzymes is in the cleavage mechanism. Lytic transglycosylases form a 1,6-anhydromuramic acid product by an intramolecular transglycosylation reaction while lysozymes in general perform a hydrolysis reaction.³ However, lysozyme from bacteriophage lambda (λ lysozyme) cleaves the peptidoglycan without the intervention of a water molecule. This mechanism therefore differs from that observed with most of the lysozymes and makes λ lysozyme a lytic transglycosylase.⁴

The active site of λ lysozyme is located between an upper and a lower domain (Figure 1). The upper domain contains four α helices ($\alpha 1$, $\alpha 4$, $\alpha 5$ and $\alpha 6$) and a long loop region that forms the upper lip. The lower domain is made up of a helix ($\alpha 2$) and a β -sheet region ($\beta 1-6$) with loops. The two domains are connected by helix $\alpha 3$. The crystal structure of the apo form of the enzyme (PDB ID:1AM7⁵) contains three molecules in the unit cell; one of them (chain B) is in a closed conformation and the other two (chains A and C) are open. The main differences between these conformations are the positions of the upper (residues 128-141) and the lower (residues 51-60) lip regions (Figure 1A). In the open conformation of the enzyme, the active-site cleft is wide open, while in the closed conformation the upper lip moves towards the lower domain restricting access to the active-site cleft. The $\alpha 6$ helix partly unwinds in the closed conformation; this makes the upper lip region longer which enables it to further cover the active-site region. NMR studies and MD simulations^{6,7} of the apo form of λ lysozyme have shown that in solution, rather than adopting either the open or closed structure, λ lysozyme populates an ensemble of conformations resulting from the dynamic nature of the upper and lower lip regions. The NMR data for apo λ lysozyme show that in solution it populates the open conformation more than the closed conformation.

A crystal structure of λ lysozyme in complex with hexa-N-acetylchitohexaose (NAG6), an inhibitor, has been determined (PDB ID: 3D3D⁸, Figure 1B). The crystallographic unit cell of this structure contains two molecules of λ lysozyme (chains A and B) (Figure S1). Both molecules have a similar structure to the closed molecule of the apo form of the enzyme. The

active site of lysozyme is traditionally divided into six subsites, A-F, where each subsite can be occupied by one sugar unit. In the crystal structure of the complex of λ lysozyme with NAG6 there are two NAG6 molecules within the unit cell. The NAG6 unit of molecule A binds to both protein molecules; it occupies the first four subsites (A-D) of protein molecule A and the last two subsites (E' and F') of the non-crystallographically related neighbouring protein molecule B (Figure 1B). This structure, which lacks a glycosidic bond across the D-E' subsites, potentially represents the products of the cleavage reaction.

In this work we have used experimental NMR studies and MD simulations to study the interaction of NAG4 and NAG6 with λ lysozyme in solution. It has been shown previously that NAG4 and larger NAG polymers are able to act as competitive inhibitors of the cleavage reaction of the natural substrate peptidoglycan.⁸ Our work enables us to investigate different possible sugar binding subsites within λ lysozyme that could be occupied prior to and during catalysis and the effects of sugar binding on the dynamics of the protein. Using the insights gained from the NMR and MD studies, the complex of λ lysozyme with the natural peptidoglycan substrate has been modelled.

Materials and Methods

NMR titrations: ¹⁵N-labelled λ lysozyme was expressed and purified as described previously.⁹ NMR experiments were performed at a λ lysozyme concentration of 0.24 mM in a 95% H₂O/5% D₂O sodium phosphate buffer at pH 4.6 and 20 °C. HSQC spectra were collected using home-built spectrometers controlled with GE/Omega software and equipped with Oxford Instruments Company magnets and home-built triple-resonance pulsed-field-gradient probeheads. Titrations with NAG4 and NAG6 were carried out at ¹H operating frequencies of 500.10 and 750.04 MHz, respectively. The data sets were acquired using 128 complex t₁ increments with ¹⁵N sweep widths of 1515.15 and 2272.73 Hz at ¹⁵N frequencies of 50.68 and 76.01 MHz, respectively. 1K complex data points were recorded in the F₂ dimension with sweep widths of 7142.86 and 10526.32 Hz at 500 and 750 MHz, respectively. 80 and 96 scans were collected per t₁ increment for the HSQC experiments at 500 and 750 MHz, respectively. The NMR spectra in the presence of NAG4 and NAG6 were assigned and analysed using CcpNmr Analysis¹⁰ using resonance assignments for λ lysozyme published previously (BMRB 16664).⁹

The interaction of λ lysozyme with NAG4 and NAG6 was monitored using 2D ^1H - ^{15}N HSQC spectra. NAG4 and NAG6, derived by the hydrolysis of crab shell chitin, were purchased from Seikagaku Corporation. The first titration was carried out using NAG6, the inhibitor used in the X-ray crystallography studies.⁸ Titration data for NAG6 were collected at concentrations of up to 6mM in 1mM increments. Concentrations above ~6mM were not possible due to the limited solubility of the NAG6. In order to achieve higher inhibitor concentrations and to investigate the binding mode of a shorter inhibitor, a second set of titration experiments was collected using NAG4. For the NAG4 titrations, lower initial concentrations of NAG4 were used, in the light of the significant broadening of peaks in the 1mM NAG6 spectrum, and higher NAG4 concentrations were achievable due to the higher solubility of NAG4 (concentrations were 0, 0.2, 0.4, 0.6, 0.8, 1.2, 2.0, 3.0, 4.2, 6.2, 9.0, 12.4, 16.2, 26.0 mM).

Chemical Shift Perturbation and Dissociation Constant Calculation: The combined $^1\text{H}^{\text{N}}$ and ^{15}N chemical shift difference (δ) was calculated for each residue using the standard equation ($\delta = \sqrt{\frac{1}{2}[\delta_H^2 + (\alpha\delta_N)^2]}$); the ^{15}N shift changes were scaled by a factor of $\alpha = 0.15$ compared to the $^1\text{H}^{\text{N}}$ chemical shift changes.¹¹ For the calculation of the dissociation constant the combined chemical shift difference is described as a function of the total sugar concentration (L_T) by

$$\Delta\delta_{obs} = \frac{\Delta\delta_{max}}{2P_T} (K_d + L_T + P_T) - \sqrt{(K_d + L_T + P_T)^2 - 4L_T P_T} \quad (1)$$

where P_T is the total protein concentration, K_d is the dissociation constant and $\Delta\delta_{max}$ is the maximum observed chemical shift difference. In the K_d calculations, the average of the combined chemical shift changes from the residues showing evidence of hydrogen bonding interaction detected from both the simulations and the NMR experiments were used. Neighbouring residues that showed significant changes through inductive effects were also included. When all the subsites were considered, the residues used in the K_d calculations were 19, 20, 68, 69, 73, 77, 98, 101 and 102. To decide which combined chemical shift changes are large enough to be considered significant indicators of the binding site, the method from Schumann et al.¹² was used.

Molecular dynamics simulations: MD simulations of λ lysozyme were performed using the GROMOS11 biomolecular simulation package (<http://www.gromos.net>)¹³ and the 5A8

GROMOS force field.¹⁴ The carbohydrate content of the complex was parametrized with the 53A6glyc parameter set¹⁵ of the GROMOS force field for carbohydrates. Parameters for the N-acetyl group in NAG have been adjusted to the current protein force field previously.¹⁶ For the modelling of the initial conformations, two crystal structures of λ lysozyme with PDB ID: 3D3D⁸ (molecule B) and 1AM7⁵ (molecule A) were used as closed and open conformations, respectively. The initial structure of the hexasaccharide bound to the closed λ lysozyme was modelled by using the crystallographic NAG6 conformation for sugars 1-4 which occupy subsites A to D. The tetrasaccharide was then extended by adding two NAG units with PyMOL.¹⁷ While adding these two NAG residues, the glycosidic angles at the linkage were set according to their most favourable energetic state with ϕ , ψ angles of -84° , 102° which have been identified previously.¹⁶ This places the final two sugar units 5-6 into subsites that we refer to as E and F while the subsites populated by the second NAG6 molecule in the crystal structure are referred to as E' and F' (Figure 1B). It is not possible to place the final two sugar units in the E' and F' sites whilst retaining a low-energy covalent bond between sugar 4, in site D, and sugar 5, in site E'. For the modelling of the open structure, molecule A from the crystal structure with PDB ID: 1AM7⁵ was aligned on the structure of closed λ lysozyme with NAG6 bound.

In addition to the complexes of open and closed λ lysozyme with NAG6, complexes of λ lysozyme with NAG4 were modelled. Due to the availability of the six subsites, four simulations of the λ lysozyme-NAG4 complex system were run, all starting from an open conformation of λ lysozyme. In the different initial structures used for these simulations the sugars occupy subsites ABCD, BCDE, CDEF and C'D'E'F'. Here, E' and F' subsites refer to the subsites which were observed in the crystal structure, as described above. When the last two sugars were fitted to the E' and F' subsites, the first two sugars needed to be shifted from subsites C and D to subsites we refer to as C' and D' in order to adopt glycosidic angles with favourable energies.

During the structure determination, all the Trp residues in the 1AM7 crystal structure were replaced by aza-tryptophans. These were changed to Trp residues for the simulations. Hydrogen atoms were added according to geometric criteria followed by a short energy minimization *in vacuo* using the steepest-descent algorithm. Each protein complex with its oligosaccharides was solvated with SPC water¹⁸ in a periodic cubic box with a minimum

protein-to-wall distance of 1.4 nm. 8 Cl⁻ ions were added to make the system charge neutral. Systems were further relaxed by a steepest descent minimization with position restraints on the solute atoms. For the equilibration, initial random velocities of all atoms were assigned from a Maxwell-Boltzman distribution at 60 K, and the system was heated up to 300 K by increasing the temperature of the external bath by 60 K every 20 ps while simultaneously, position restraints on the solute atoms were reduced from 2.5×10^4 to 0.0 kJ mol⁻¹ nm⁻². All the simulations were performed at a constant temperature of 300 K and a constant pressure of 1 atm using a weak coupling scheme¹⁹ for both temperature and pressure with coupling times $\tau_T = 0.1$ ps and $\tau_P = 0.5$ ps and an isothermal compressibility of 4.575×10^{-4} kJ⁻¹ mol nm³. For all production runs, a leapfrog integration scheme²⁰ with a time step of 2 fs was used, and covalent bonds were constrained to maintain the optimal bond length. Nonbonded interactions were computed using a pairlist²¹ that was updated every 5 steps. Interactions up to 0.8 nm were computed at every timestep and up to 1.4 nm were computed at pairlist updates and kept constant in between. Long-range electrostatic interactions beyond a cutoff of 1.4 nm were truncated and approximated by a generalized reaction field²² with a dielectric permittivity of 61.²³ The SHAKE algorithm²⁴ was used to maintain the bond lengths.

For the clustering and time series analysis the GROMOS++ software²⁵ was used. The DSSP program²⁶ was used to identify the regions of secondary structures of the conformers within the simulations. For the hydrogen bond analysis, a geometrical criterion was used where hydrogen bonds are identified if the hydrogen-acceptor distance is smaller than 0.25 nm and the donor-hydrogen-acceptor angle is larger than 135°. Conformational clustering was performed based on pairwise root-mean-square differences between configurations, using a cutoff of 0.35 nm to identify structural neighbours.²⁷

Results and Discussion

NMR Chemical Shift Perturbations

The binding of tetra-NAG (NAG4) and hexa-NAG (NAG6) to λ lysozyme in solution was characterized, at a residue-specific level, using NMR methods. 2D ¹H-¹⁵N HSQC spectra were recorded and analysed for λ lysozyme in the presence of different concentrations of NAG6 (0-6mM) and NAG4 (0-26 mM); a region of the HSQC spectra is shown in Figure 2. The changes in backbone and side chain ¹H^N and ¹⁵N chemical shifts and peak intensities were followed through the titrations (Figures 3). Residues without significant chemical shift

changes in the presence of 6mM NAG (such as Val35 and Lys 145 in Figure 2) also showed no significant change in peak shape in the presence of NAG6. This suggests there is no increase in the rotational correlation time indicating that, in solution, the sugar molecules do not cross-link two λ lysozyme molecules as is seen in the crystal structure of the λ lysozyme - NAG6 complex.⁸

The spectrum of λ lysozyme in the presence of NAG6 shows peak broadening of specific residues in addition to changes in chemical shifts (Figures 2 and 3); approximately 10 residues are broadened beyond detection with the first addition of ~1mM NAG6 (Figure 3C) and these cannot be followed during the titration. In the NAG4 titration, smaller additions of the sugar were made allowing more residues to be followed during the course of the titration. A comparison of the loss in peak intensity in the presence of ~1mM NAG4 and NAG6 shows similar patterns of broadening across the λ lysozyme sequence for the two sugars. A comparison of the spectra shown in Figure 2 for the NAG4 and NAG6 titrations also shows that peaks shift in the same way in the two series of spectra. The combined backbone $^1\text{H}^\text{N}$ and ^{15}N chemical shift changes for λ lysozyme in the presence of ~ 6 mM NAG4 and NAG6 are shown as a function of sequence in Figure 3. For the majority of residues, shifts of similar magnitude were observed in the two titrations (Figure 3) suggesting that the two sugars bind to λ lysozyme in a similar manner. The broadening and shifts observed for residues including Glu101, Asn122, Leu70, Ala125, Glu19 and Gly20 suggest interactions of NAG4/NAG6 in the A, B, C, D, E and F sites, respectively. Chemical shift changes observed for NAG4 concentrations ranging from 0.2mM to 26mM allow the dissociation constant to be determined using standard methods. This was calculated to be ~6mM (Figure S2). The titrations with NAG6 show a similar pattern of chemical shift changes suggesting a similar K_d value.

Analysis of Peak Broadening

The most significant broadening of peaks is observed for residues at the C-terminus of λ lysozyme (Figure 3C). Addition of 1mM NAG6 leads to broadening beyond detection of the peaks corresponding to residues Asn122, Trp124, Ser126, Ala130, Ala139 and Asp140. The crystal structure of the NAG6 - λ lysozyme complex shows that Asn122, Ile123, Ala125 and Phe135 are involved in direct hydrogen bond interactions with sugars in the B, C, D and E sites, respectively. In addition, Trp124, Ser126, Tyr132 and Gln134 are within 0.4 nm of

sugars in the C, D and E sites. Therefore, some of the observed broadening is likely to arise from these direct interactions. Interestingly, residues 139 and 140, which are completely broadened, and neighbouring residues 138 and 141, which are significantly broadened, do not make contacts with the sugar moieties. However, these residues are significantly perturbed both by large displacements in the structure and by changes in hydrogen bonding interactions between the open and closed structures of the protein.⁵ For example, the H^N of Lys138, Ala139 and Asp140 are hydrogen bonded to the CO of Gln134, Phe135 and Glu136, respectively, in the open structure but not in the closed one. Thus, some of the observed peak intensity perturbations for C-terminal residues may indicate a change in the population of open and closed structures, or in the dynamics of their interconversion, as NAG4/NAG6 bind to λ lysozyme.

Molecular dynamics simulations

MD simulations of λ lysozyme in complex with NAG4 and NAG6 were used to provide structural models for the complex and to characterise the dynamics of the protein complex. Different conformations of λ lysozyme seen in crystallographic studies were used as starting structures for the simulations to capture a dynamic picture of the enzyme. Two 150 ns simulations of λ lysozyme in complex with NAG6 were performed starting from the open and closed conformations of λ lysozyme (Figure 1C; simulations NAG6_1 and NAG6_2 respectively). As discussed above, in the crystal structure subsites ABCD in λ lysozyme are occupied by one NAG6 molecule while the final two subsites are occupied by a second NAG6 molecule from a non-crystallographically related neighbouring molecule. For the simulations, the initial structure of the hexasaccharide was modelled by using the crystallographic NAG6 conformation for sugars 1-4 which occupy subsites A to D and then adding the two final sugar units with a linkage conformation corresponding to the lowest free energy. This places the final two sugar units 5-6 into subsites that we refer to as E and F while the subsites populated by the second NAG6 molecule in the crystal structure are referred to as E' and F' (Figure 1B). It is not possible to place the final two sugar units in the E' and F' sites whilst retaining a low-energy covalent bond between sugar 4, in site D, and sugar 5, in site E'. The free-energy landscape of the glycosidic linkage is illustrated in Figure 4A⁹ with the glycosidic dihedral angles of the NAG6 units in the bound crystal structure shown in black, populating the lowest energy state. During simulation NAG6_1, a change in the orientation of the linkage between the sugar units populating the D and E subsites was

observed (Figure 4E). This change in the glycosidic dihedral angle allows the movement of the sugars 5 and 6 towards the upper domain, populating new positions which we refer to as sites E^u and F^u. This change is not observed when the protein adopts the closed conformation and so different interactions with the protein are seen for sugars 5 and 6 in the simulations starting from the open and closed states of λ lysozyme.

Four 150 ns simulations of λ lysozyme in complex with NAG4 starting from the open conformation of λ lysozyme were performed. In these four simulations the sugar occupied binding subsites ABCD, BCDE, CDEF, and C'D'E'F' in the starting structure (Figure 1D; simulations NAG4_1 to 4, respectively) where EF and E'F' are the subsites populated when the lowest free-energy glycosidic linkage is adopted and those populated in the crystal structure, respectively. When the last two sugars were fitted into the E'F' subsites it was not possible to place the first two sugars in the C and D subsites. Therefore, the C'D'E'F' model was created by populating the E'F' subsites and setting the D'-E' glycosidic angle to its lowest energy state (NAG4_4). The C'D' subsites were shifted compared to those in the crystal structure as can be seen in Figure 1D. A similar binding mode is seen in the complex of Ra-ChiC, a lysozyme-like chitinolytic enzyme, with NAG4 (PDB ID 3W6C²⁸; Figure S3) which has the highest sequence similarity among the structural representatives of λ lysozyme²⁹⁻³¹ in the Protein Data Bank (PDB, www.rcsb.org³²).

The total non-bonded interaction energy (van der Waals and electrostatic) between the individual sugars and the protein were compared in the four NAG4 simulations (Figure S4). For the NAG4_1 simulation, the highest contributions are from subsite A (-194 ± 6 kJ/mol) and subsite C (-128 ± 1 kJ/mol) with a total non-bonded interaction energy of -499 ± 9 kJ/mol. The sugar binding to λ lysozyme in the NAG4_2 simulation was not stable as the sugar dissociated from the active site after 100 ns (Figures S5D in the supplementary material), the apo enzyme then adopting a closed conformation (Figure S5C). Prior to the loss of the sugar the total non-bonded interaction energy was approximately -300 kJ/mol with most of the contributions coming from subsites B and C. In the NAG4_3 simulation, the total interaction energy is -401 ± 19 kJ/mol with the largest contribution coming from sugar 3 in subsite C (-149 ± 6 kJ/mol). In this simulation after 40 ns a similar change in the orientation of the linkage between the sugar units populating the D and E subsites is observed as is seen in the simulation NAG6_1 (compare Figures 4C and 4E). This makes the final two sugars more flexible and the total interaction energy increases as the final sugar starts to form

hydrogen bonds with Gln 134 in the upper lip region populating sites E^u and F^u (Figure 5D and S5F). In simulation NAG4_4 the total interaction energy is -545 ± 8 kJ/mol with the greatest contribution coming from the sugar in subsite E' (-219 ± 7 kJ/mol). In this case the E'F' subsites are right under the upper lip and the D'-E' linkage is making a close contact with the active site. In this simulation after approximately 70 ns the total interaction energy dropped to -300 kJ/mol but it then increased again. This behaviour can be explained by the rearrangement of the lower lip region as can be seen from Figure S6. After rearrangement the sugar in sites C' and F' make a favourable interaction resulting in an increase in the total interaction energy. Comparison of all the simulations of λ lysozyme with NAG4 suggests that NAG4 may bind in subsites ABCD, CDEF and transiently in subsites C'D'E'F' but not in subsites BCDE. It is interesting that the highest contributions to the interaction energy consistently correspond to the A, C and E sites to which NAG binds in the natural NAG/NAM substrate.

In both the NAG6_1 and the NAG4_3 simulations there is a similar change in orientation of the D-E linkage between the sugar units populating the D and E subsites. There is considerable interest in the ligand-binding modes in subsites D and E since the catalysis of the cleavage of the $\beta(1 \rightarrow 4)$ glycosidic bond happens between these two subsites. We identify here changes at the glycosidic linkage at these subsites which enable the adoption of other energetically favourable states during the MD simulation in Figure 4. In the second energetically favourable state, the sugar makes favourable hydrogen bonding contacts with residues in the upper lip region of the protein.

λ lysozyme showed different conformational states in the MD simulations, especially in the upper and lower lip regions. To characterise this, the distance between the upper lip (Tyr132: C α) and lower lip (Lys58: C α) and their distances to the catalytic residue Glu19, which is located between them, was calculated to assess the contribution of each lip region to the opening and closing mechanism of the protein (Figures S5, S6 and S8). In addition, all the conformers of λ lysozyme from the six MD simulations were clustered: clusters 1 and 2 correspond to the open and closed conformations of λ lysozyme, respectively, and clusters 3, 4 and 5 represent conformations which are in between open and closed configurations (Figure S7). In the NAG4 simulations, which were started from the open configuration, the protein was either in the open configuration or populated conformations which are in between open

and closed but the structure did not completely close. For the NAG6_1 simulation, which was started from the open conformation, almost half the conformers belong to cluster 2, indicating a closed state. The other half of the frames were distributed between the rest of the clusters indicating that the protein was closing and opening during the simulation as illustrated by the distances in Figure S8. The protein remains closed in the NAG6_2 simulation, indeed closing further than the closed crystal structure (Figure S8). A superimposition of the structures from the central members of the clusters showed that during opening of the structure there are changes to the $\alpha 6$ helix region (Figure S9A).

Comparison of the NMR data, MD simulations and crystal structures

The combined $^1\text{H}^{\text{N}}$ and ^{15}N chemical shift changes in the NAG4 and NAG6 NMR titrations were mapped on to the λ lysozyme complex conformations populated during the different simulations (Figure S10). On the basis of the MD simulation results we make the assumption that NAG4 can occupy both the ABCD subsites and the CDEF subsites and so in the NMR experiments we see an average which corresponds to all the subsites being occupied to some extent. To simplify the comparisons, the chemical shift data from both the NMR titration experiments were compared with the NAG6 simulations. Significant chemical shift changes or resonance broadening could reflect changes in chemical environment due to the proximity of the sugar, hydrogen bonding to a sugar unit, the presence of multiple conformations, or changes to the dynamics of the protein as a result of the sugar binding. Overall, the residues whose chemical shifts are most affected by the sugar binding surround the active-site cleft.

Table S1 identifies hydrogen bonds between λ lysozyme and NAG6 in the crystal structure and also hydrogen bonds between the enzyme and the sugar in the two simulations of the λ lysozyme-NAG6 complex (open and closed) and compares them with the overall chemical shift changes seen in the NAG4 and NAG6 titrations. A similar pattern of hydrogen bonding is also observed in the NAG4 simulations (Figure 5). Table S1 shows that all the residues that show direct interactions with the sugar in the crystal structure or simulations either broaden beyond detection or have a significant chemical shift change during the titrations. High hydrogen bonding populations were observed in either or both an open and closed simulation between the sugars in subsites B, C, D and λ lysozyme, particularly involving residues Leu70, Gln98, Asn122, Ile123 and Ala125 (and also the side chain of Tyr 77). These residues are also involved in hydrogen bonding interactions in the crystal structure of the λ lysozyme-

NAG6 complex. The backbone resonances of Leu70, Asn122, Ile123 and Ala125 and the side chain of Gln98, all broaden beyond detection during the NAG4 and NAG6 titrations. The resonances of the Asn122 side chain protons also shift significantly.

As discussed above, flexibility of the linkage between the sugars occupying subsites D and E was identified in some of the simulations causing the final two sugar units to adopt alternative conformations populating subsites E^u and F^u. The population of these alternative subsites, in addition to the E and F subsites, is supported by the results of the NMR titrations. Some of the residues with which the sugar units in subsites E^u and F^u interact show either significant chemical shift changes or their resonances broaden and disappear from the spectra. The largest effect is seen for Gly133 which showed a combined chemical shift change of 0.150 ppm in the NAG4 titration and in the NAG6 titration its resonance broadened and disappeared. This residue also makes hydrogen bonding interactions with the last sugar (F^u) as illustrated in Figure 5D.

When a carbonyl group forms a hydrogen bond to the sugar, the largest effect is often seen for the amide group of the following residue rather than the amide group of the same residue. This is seen, for example, for residue Gln68 where its backbone oxygen is involved in hydrogen bonding in the simulations. Its overall backbone shifts were 0.079 and 0.096 ppm while the following residue, Leu69, showed larger shifts of 0.114 and 0.161 ppm in the NAG4 and NAG6 titrations, respectively. Interestingly, in the crystal structure Gln68 hydrogen bonds to the sugar using its side chain oxygen, not its backbone carbonyl oxygen.

The region with the most significant broadening during the titrations is the upper lip region (residues 128-141). Some of the residues in this region, Tyr132 and Phe135, interact with the ligand in both the MD simulations and the crystal structure of the complex. It was noted earlier that some of the broadened residues do not make contact with the sugar in the crystal structure; contacts between these residues and the sugar are also not observed in the MD simulations. The broadening and disappearance of resonances for these residues in the upper lip region may therefore reflect changes in the population and dynamics of the multiple conformations this region samples in solution in the presence of inhibitor.

The chemical shift changes observed for the NAG4 and NAG6 titrations are generally similar although there are some interesting differences (Figure 3). Many of the residues that make

contact with sugars in sites C and D show shifts of similar magnitudes for the two sugars; examples of this include Lys60, Leu69, Ile123 and Ala125. Interestingly, the shifts observed for Tyr77, Glu101 and Arg102 are smaller in the NAG4 titration than in the NAG6 titration; these residues make contact with sugars in the A and B sites. A similar pattern is observed for residues Ser18, Gly20, Ser26 and Phe135, which make contact with sugars in the E and F sites. NAG6 will occupy sites A-F while NAG4 occupies either ABCD or CDEF. Therefore, in the NAG4 titration, the AB and EF sites are not fully occupied in contrast to the CD sites; this correlates well with the observed shift changes.

Modeling of the λ lysozyme - peptidoglycan complex

Although there have been many studies of the chemical structure of peptidoglycans, there is no consensus on the preferred 3D molecular structure adopted or its arrangement in the cell wall.³³⁻³⁷ While the glycan backbone of peptidoglycan is conserved in all bacteria with alternating NAM and NAG units with a $\beta(1-4)$ linkage, the peptide moiety shows diversity. Most of the NAM residues in the peptidoglycan are substituted with a pentapeptide of general sequence L-Ala¹- γ -D-Glu²-L-Lys³-D-Ala⁴-D-Ala⁵. However, the residue at position 3 is replaced by diaminopimelic acid in Dap-type peptidoglycan which is mostly seen in Gram-negative bacteria. Here, we modeled a peptidoglycan octamer with a NAG-NAM(-L-Ala- γ -D-Glu-L-Dap-D-Ala-D-Ala) disaccharide repeating unit since λ lysozyme has been shown to be more active for gram-negative bacterial cell wall lysis.³⁸ According to theoretical and experimental analysis, the glycosidic dihedral angles of the NAM- $\beta(1-4)$ -NAG unit are similar to a NAG- $\beta(1-4)$ -NAG unit (chitin-like structure) whereas the conformational map is more restricted in a NAG- $\beta(1-4)$ -NAM unit.³⁷ Therefore, we used the $\phi, \psi : -84^\circ, 102^\circ$ glycosidic angles for the NAM-NAG disaccharide, which have been previously determined from free-energy calculations.¹⁶ Glycosidic angles for the NAG-NAM disaccharide were taken from the NMR structure of a peptidoglycan monomer fragment³⁶ ($\phi, \psi : -62^\circ, 118^\circ$ where ϕ is the O5-C1-O4-C4 dihedral and ψ is the C1-O4-C4-C3 dihedral). The pentapeptide conformation seen in the NMR structures of the unbound peptidoglycan monomer, dimer and protein-bound peptidoglycan polymers show that it is not well-defined.^{35,36,39-41} We attached the pentapeptide to each NAM unit with dihedral angles of 30° for C2-C3-O3-C9 and 60° for O3-C9-C10-N2 as seen in the NMR structure of the peptidoglycan dimer. After building the NAG1-NAM1(-P1)-NAG2-NAM2(-P2)-NAG3-NAM3(-P3)-NAG4-NAM4(-P4) unit, energy minimization was applied in the λ lysozyme active site using the open conformation of the

protein. Upon minimization, the glycosidic dihedral angles of the glycan portion did not change significantly but the pentapeptide moieties of the NAM residues showed changes in conformation.

As can be seen from the molecular surface representation (Figure 6A), after the minimization of the modelled peptidoglycan structure, the glycan portion filled the extended active-site groove. Most of the pockets with polar sites on the protein surface identified in the MD simulations of λ lysozyme with NAG4 or NAG6, in addition to the active-site groove, are now occupied by the peptide portion of the peptidoglycan (Figures S11 and S12). All the peptide units show favourable hydrogen bonding patterns with residues found to be important in interactions with the sugars in the simulations (Figures 6, S11, S12). Peptide moiety P3, which is in close proximity to the active site, showed strong hydrogen bonding with three residues: Ile123, Ala125 and Gln134. Interestingly, these are some of the residues which were driving the NAG6 and NAG4 sugars (without peptide chains), in the simulations NAG6_1 and NAG4_3, towards the pocket containing the E^u and F^u sugar binding sites when the structure was open. Our λ lysozyme - peptidoglycan model suggests that in the presence of the natural substrate this E^uF^u pocket will be occupied by the peptide moiety and the sugars occupy the EF or E'F' subsites. In addition to that, our model suggests that the peptide moiety P4 binds adjacent to the λ lysozyme lower lip region. Here there was a significant loss of secondary structure in the β 3- β 4 strands (residues 52-56 and 59-61) during the simulations. However, the model suggests that hydrogen bonding interactions between the peptide moiety P4 and Lys60 and Ser61 in λ lysozyme may stabilize the secondary structure in the lower lip in the complex with peptidoglycan. The additional interactions between these peptide moieties and λ lysozyme are likely to be responsible for the higher affinity of the enzyme for its natural substrate.

Notably, a previous structural alignment of lysozyme from T4 bacteriophage (T4L) with a dimer portion of peptidoglycan⁴⁰ identified a similar interaction pattern between the peptidoglycan and protein close to the enzyme active site. Superimposing these structures demonstrates that the peptide moiety of peptidoglycan that makes key interactions with the T4L enzyme, occupies similar binding sites to those observed in our model of the λ lysozyme complex with the peptidoglycan octamer (Figure 6A).

Conclusion

NMR studies and MD simulations have given a consistent picture of the binding of NAG4 and NAG6 to λ lysozyme in solution. Residues particularly in subsites B, C and D of λ lysozyme make persistent hydrogen bonds to the sugar units, while flexibility in the D-E linkage enables the final two sugar units to explore a number of binding modes including the EF, E'F' and E^uF^u subsites. The D-E linkage is in the vicinity of the catalytic residue Glu19 and this is the site where cleavage of the glycosidic bond occurs during catalysis. The combination of persistent hydrogen bonding between the sugar and protein, but with flexibility around the D-E linkage, may be essential features for the activity of the enzyme. Our λ lysozyme - peptidoglycan model suggests that in the presence of the natural substrate the E^u-F^u pocket will be occupied by the peptide chains while the sugars occupy the E-F or E'-F' subsites. This would hold the substrate in place whilst allowing a conformational change at the active site. In light of this behaviour it is interesting that in the crystal structure of the complex of λ lysozyme with NAG6, a single sugar molecule does not occupy all six subsites in a single molecule of λ lysozyme. In molecule A of λ lysozyme subsites A-D are populated by four of the NAG6 units and subsites E'F' are populated by a second NAG6 molecule. Therefore, the D-E linkage, which is flexible in the simulations, is missing in both the molecules in the crystal structure.

Previous NMR studies and MD simulations of λ lysozyme have identified that in the apo state in solution the upper and lower lip regions of the protein are flexible. In the crystal structure of the complex of λ lysozyme with NAG6 both molecules adopt a closed conformation. However, in all the MD simulations of the λ lysozyme complexes reported here, which were started from different conformations of the enzyme and with different sugar binding modes, the upper and lower lip regions are dynamic allowing the enzyme to adopt both open and closed conformations. In addition, in the NMR titrations of λ lysozyme with NAG4 and NAG6 significant broadening of the resonances of residues within the upper lip region is observed although some of these residues are not close to the ligand binding site. This suggests that the flexibility of the lip regions seen for the apo protein in solution is maintained, to some extent, in the complex although there may be changes to the timescale or nature of the dynamics. Our results suggest that an open form is needed for the entry of the substrate and upon ligand binding the upper and lower lips retain flexibility but can close to create a cage around the catalytic Glu19 as required for the activity of the enzyme. This study

demonstrates that NMR spectroscopy combined with molecular dynamics simulations can provide information that is complementary to the static crystal structure by highlighting the dynamic nature of the enzyme-inhibitor complex.

Acknowledgements

A.T. and C.O. thank the Austrian Science Fund (FWF) for financial support through the Biomolecular Technology of Proteins (BioToP) doctoral program, grant number W1224. A.M. was supported in part by the Fonds de la Recherche Fondamentale Collective (FRFC, grant number 2.4530.09) and A.D.P. was the recipient of a F.R.I.A. PhD fellowship. A.M. and C.R. acknowledge support from the Belgian program of Interuniversity Attraction Poles, initiated by the Federal Office for Scientific Technical and Cultural Affaires (PAI n8 P7/44). C.R. acknowledges support from the Wellcome Trust (Grant No. 079440). L.J.S. would like to acknowledge the use of the University of Oxford Advanced Research Computing (ARC) facility in carrying out some of this work. <http://dx.doi.org/10.5281/zenodo.22558>.

Supporting Information

Additional supporting information may be found online in the Supporting Information section at the end of this article.

References

1. Jolles P. *Lysozymes: Model enzymes in biochemistry and biology*. Birkhauser Verlag, Basel; 1996.
2. Vollmer W, Joris B, Charlier P, Foster S. Bacterial peptidoglycan (murein) hydrolases. *Fems Microbiol Rev*. 2008;32:259-286.
3. Holtje JV. From growth to autolysis - the murein hydrolases in *Escherichia-Coli*. *Arch Microbiol*. 1995;164:243-254.
4. Bienkowskaszewczyk K, Lipinska B, Taylor A. The R-gene product of bacteriophage lamda is the murein transglycosylase. *Molecular & General Genetics*. 1981;184:111-114.

5. Evrard C, Fastrez J, Declercq JP. Crystal structure of the lysozyme from bacteriophage lambda and its relationship with V and C-type lysozymes. *J Mol Biol.* 1998;276:151-164.
6. Smith LJ, Bowen AM, Di Paolo A, Matagne A, Redfield C. The dynamics of lysozyme from bacteriophage lambda in solution probed by NMR and MD simulations. *Chembiochem.* 2013;14:1780-1788.
7. Smith LJ, van Gunsteren WF, Hansen N. Characterization of the flexible lip regions in bacteriophage lambda lysozyme using MD simulations. *Eur Biophys J.* 2015;44:235-247.
8. Leung AKW, Duewel HS, Honek JF, Berghuis AM. Crystal structure of the lytic transglycosylase from bacteriophage lambda in complex with hexa-N-acetylchitohexaose. *Biochemistry.* 2001;40:5665-5673.
9. Di Paolo A, Duval V, Matagne A, Redfield C. Backbone H-1, C-13, and N-15 resonance assignments for lysozyme from bacteriophage lambda. *Biomol NMR Assign.* 2010;4:111-114.
10. Vranken WF, Boucher W, Stevens TJ, et al. The CCPN data model for NMR spectroscopy: Development of a software pipeline. *Proteins.* 2005;59:687-696.
11. Williamson MP. Using chemical shift perturbation to characterise ligand binding. *Progr Nuclear Mag Reson Spectr.* 2013;73:1-16.
12. Schumann FH, Riepl H, Maurer T, Gronwald W, Neidig KP, Kalbitzer HR. Combined chemical shift changes and amino acid specific chemical shift mapping of protein-protein interactions. *J Biomol NMR.* 2007;39:275-289.
13. Schmid N, Christ CD, Christen M, Eichenberger AP, van Gunsteren WF. Architecture, implementation and parallelisation of the GROMOS software for biomolecular simulation. *Computer Physics Communications.* 2012;183:890-903.

14. Reif MM, Hunenberger PH, Oostenbrink C. New interaction parameters for charged amino acid side chains in the gromos force field. *J Chem Theory & Comp.* 2012;8:3705-3723.
15. Pol-Fachin L, Rusu VH, Verli H, Lins RD. GROMOS 53A6(GLYC), an improved GROMOS force field for hexopyranose-based carbohydrates. *J Chem Theory & Comp.* 2012;8:4681-4690.
16. Turupcu A, Oostenbrink C. Modeling of oligosaccharides within glycoproteins from free-energy landscapes. *J Chem Inf Model.* 2017;57:2222-2236.
17. *The Pymol Molecular Graphics System, Version 1.6.0.0 Schrödinger, LLC.*
18. Berendsen HJC, Postma JPM, van Gunsteren WF, Hermans J. Interaction models for water in relation to protein hydration. In: Pullman B, ed. *Intermolecular forces*. Dordrecht, The Netherlands: Reidel; 1981:331-342.
19. Berendsen HJC, Postma JPM, van Gunsteren WF, Dinola A, Haak JR. Molecular dynamics with coupling to an external bath. *J Chem Phys.* 1984;81:3684-3690.
20. Hockney RW. Potential calculation and some applications. *Methods Comput Phys.* 1970;9:135-211.
21. Heinz TN, Hunenberger PH. A fast pairlist-construction algorithm for molecular simulations under periodic boundary conditions. *J Comput Chem.* 2004;25:1474-1486.
22. Tironi IG, Sperb R, Smith PE, van Gunsteren WF. A generalised reaction field method for molecular dynamics simulations. *J Chem Phys.* 1995;102:5451-5459.
23. Heinz TN, van Gunsteren WF, Hunenberger PH. Comparison of four methods to compute the dielectric permittivity of liquids from molecular dynamics simulations. *J Chem Phys.* 2001;115:1125-1136.

24. Ryckaert JP, Ciccotti G, Berendsen HJC. Numerical integration of cartesian equations of motion of a system with constraints - molecular dynamics of n-alkanes. *J Comput Phys.* 1977;23:327-341.
25. Eichenberger AP, Allison JR, Dolenc J, et al. GROMOS ++ software for the analysis of biomolecular simulation trajectories. *J Chem Theory & Comput.* 2011;7:3379-3390.
26. Kabsch W, Sander C. Dictionary of protein secondary structure - pattern recognition of hydrogen bonded and geometrical features *Biopolymers.* 1983;22:2577-2637.
27. van Gunsteren WF, Allison JR, Daura X, et al. Deriving structural information from experimentally measured data on biomolecules. *Angew Chemie-Int Ed.* 2016;55:15990-16010.
28. Arimori T, Kawamoto N, Shinya S, et al. Crystal structures of the catalytic domain of a novel glycohydrolase family 23 chitinase from *Ralstonia* sp A-471 reveals a unique arrangement of the catalytic residues for inverting chitin hydrolysis. *J Biol Chem.* 2013;288:18696-18706.
29. Prlic A, Bliven S, Rose PW, et al. Pre-calculated protein structure alignments at the RSCB PDB website. *Bioinformatics.* 2010;26:2983-2985.
30. Andreeva A, Howorth D, Chandonia JM, et al. Data growth and its impact on the scop database: New developments. *Nucleic Acids Res.* 2008;36:D419-D425.
31. Ye YZ, Godzik A. Flexible structure alignment by chaining aligned fragment pairs allowing twists. *Bioinformatics.* 2003;19:1246-1255.
32. Berman HM, Westbrook J, Feng Z, et al. The Protein Data Bank. *Nucleic Acids Res.* 2000;28:235-242.
33. Kim SJ, Chang J, Singh M. Peptidoglycan architecture of gram-positive bacteria by solid-state NMR. *BBA-Biomembranes.* 2015;1848:350-362.

34. Schumann P. Peptidoglycan structure. In: Rainey F, Oren A, eds. *Methods in microbiology, vol 38: Taxonomy of prokaryotes*. Vol 38.2011:101-129.
35. Meroueh SO, Bencze KZ, Heseck D, et al. Three-dimensional structure of the bacterial cell wall peptidoglycan. *Proc Nat Acad Sci USA*. 2006;103:4404-4409.
36. Matter H, Szilagyi L, Forgo P, Marinic Z, Klaic B. Structure and dynamics of a peptidoglycan monomer in aqueous solution using NMR spectroscopy and simulated annealing calculations. *J Am Chem Soc*. 1997;119:2212-2223.
37. Rao R, Qasba, PK, Balaji, PV Chandrasekaran, R. *Conformation of carbohydrates*. Amsterdam, The Netherlands: Harwood Academic Publishers; 1998.
38. Nakimbugwe D, Masschalck B, Deckers D, Callewaert L, Aertsen A, Michiels CW. Cell wall substrate specificity of six different lysozymes and lysozyme inhibitory activity of bacterial extracts. *Fems Microbiol Lett*. 2006;259:41-46.
39. Cho S, Wang Q, Swaminathan CP, et al. Structural insights into the bactericidal mechanism of human peptidoglycan recognition proteins. *Proc Nat Acad Sci USA*. 2007;104:8761-8766.
40. Kuroki R, Weaver LH, Matthews BW. A covalent enzyme-substrate intermediate with saccharide distortion in a mutant T4 lysozyme. *Science (New York, NY)*. 1993;262:2030-2033.
41. Anderson WF, Grutter MG, Remington SJ, Weaver LH, Matthews BW. Crystallographic determination of the mode of binding of oligosaccharides to bacteriophage-t4 lysozyme - implications for the mechanism of catalysis. *J Mol Biol*. 1981;147:523-543.
42. *Molecular operating environment (MOE) 2013.08*. 2018.

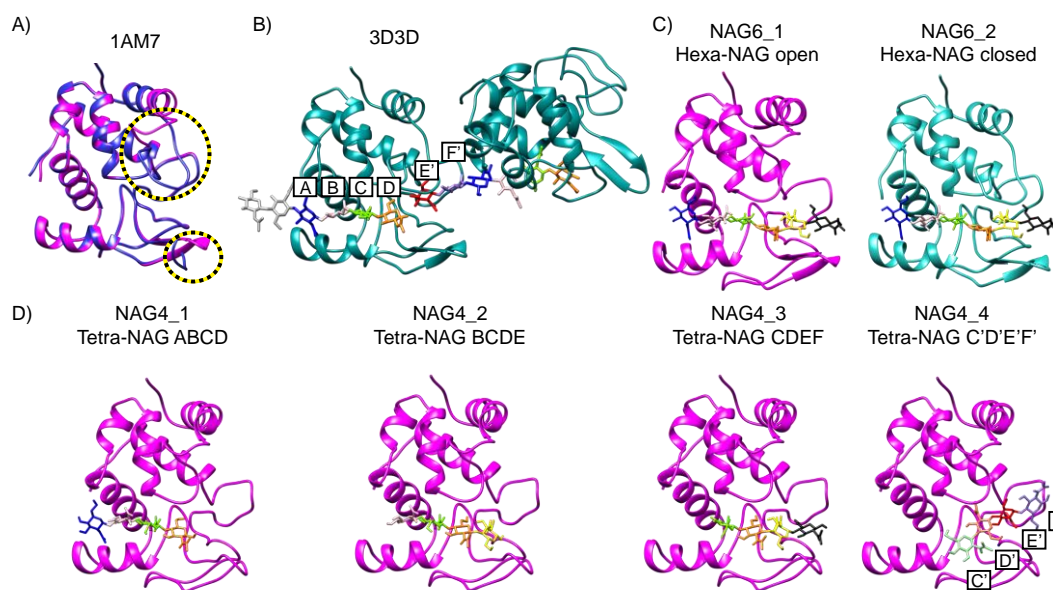


Figure 1. The structure of λ lysozyme in the available X-ray structures and the modelled initial structures used in the MD simulations. A) The X-ray structure of the apo state of λ lysozyme (1AM7). The three molecules in the asymmetric unit are shown superimposed. One of these is in the closed conformation (blue) and the other two are in the open conformation (magenta). The upper lip (residues 128-141) and lower lip (51-60) regions of λ lysozyme (indicated by yellow/black circles) show significant differences between the open and closed conformations. B) The crystal structure containing two molecules of the complex of λ lysozyme in the closed conformation with two NAG6 molecules (PDB ID: 3D3D). Each molecule is bound to its NAG6 unit using the A, B, C and D subsites and to the other sugar unit using its E' and F' subsites. C) The modelled open (magenta) and closed (cyan) NAG6-lysozyme systems used as the initial structures in the NAG6_1 and NAG6_2 simulations, respectively. Here, the 5th and 6th sugars occupy different subsites on the protein than in panel B. The model was created by keeping the first four sugars in sites ABCD and adding the 5th and 6th sugars to sites E and F with their glycosidic dihedral angles set to their lowest energy state (see Materials and Methods). D) The four different initial NAG4-lysozyme models used in the simulations with sugars occupying sites ABCD (NAG4_1), BCDE (NAG4_2), CDEF (NAG4_3), and C'D'E'F' (NAG4_4). All four simulations started from the open structure of λ -lysozyme (shown in magenta). In all panels, the sugar units are colour-coded as follows: A-blue, B-pale pink, C-green, C'-pale green, D-orange, D'-pale orange, E-yellow, E'-red, F-black, F'-lavender. Sugar units not bound to λ lysozyme are shown in pale grey in B).

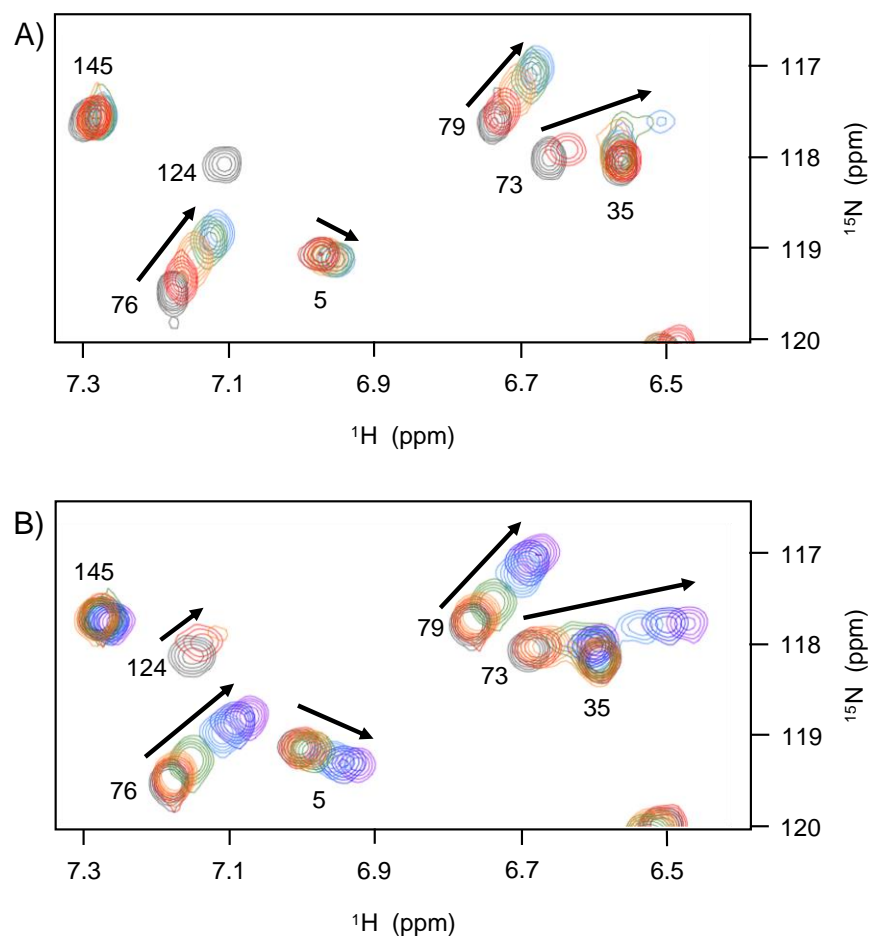


Figure 2. Superposition of a region of the ^1H - ^{15}N HSQC spectra of λ lysozyme recorded during titrations with (A) NAG6 and (B) NAG4. Peaks arising from Asn5, Val35, Trp73, Ala76, Lys79, Trp124 and Lys145 are shown. The arrows indicate the direction of the peak shifts during the course of the titrations. A) Overlaid spectra correspond to NAG6 concentrations of 0 (dark grey), 1mM (red), 2mM (orange), 4mM (green) and 6mM (blue). B) Overlaid spectra correspond to NAG4 concentrations of 0 (dark grey), 0.4mM (red), 0.8mM (orange), 2mM (green), 6mM (blue), 12.4mM (dark blue) and 26mM (purple). It can be seen that peaks shift in the same direction and to a very similar extent in the 6mM spectra for NAG6 and NAG4 shown in blue. The peak corresponding to Trp124 which disappears with 1mM NAG6 can be seen in the spectra collected with 0.4 and 0.8mM NAG4.

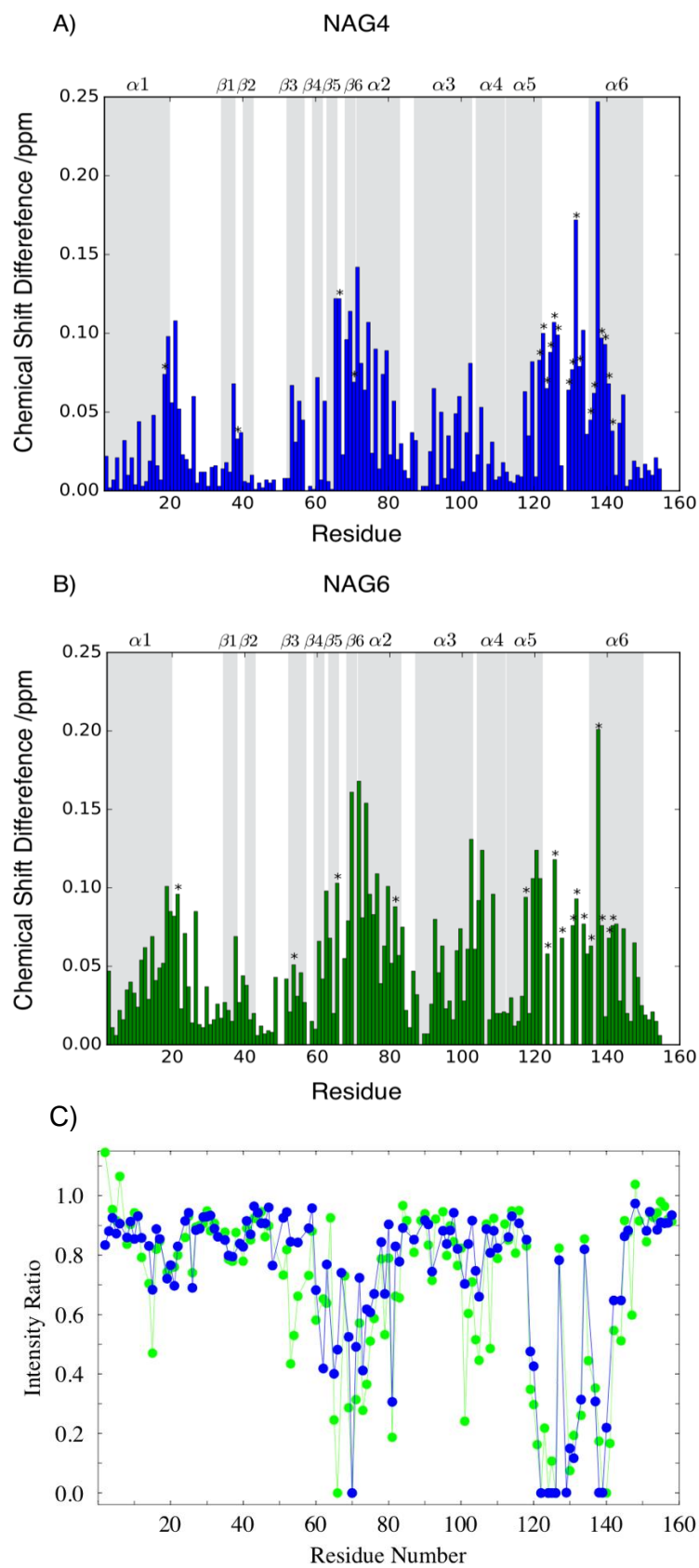


Figure 3. Comparison of chemical shift differences and peak broadening observed with NAG4 and NAG6. Combined $^1\text{H}^{\text{N}}\text{-}^{15}\text{N}$ chemical shift difference between apo λ lysozyme and λ lysozyme in complex with ~ 6 mM NAG4 (A) and ~ 6 mM NAG6 (B). The chemical shift differences of peaks that disappear from spectra have been extrapolated, where possible, using the experimental K_d value and are indicated with an asterisk. Regions of secondary structure in λ lysozyme are shown in grey and labelled at the top of each plot. (C) HSQC peak intensity for λ lysozyme observed with ~ 1 mM NAG4 (blue) or NAG6 (green) relative to intensity observed for apo λ lysozyme. Peaks that broaden beyond detection have an intensity ratio of 0.

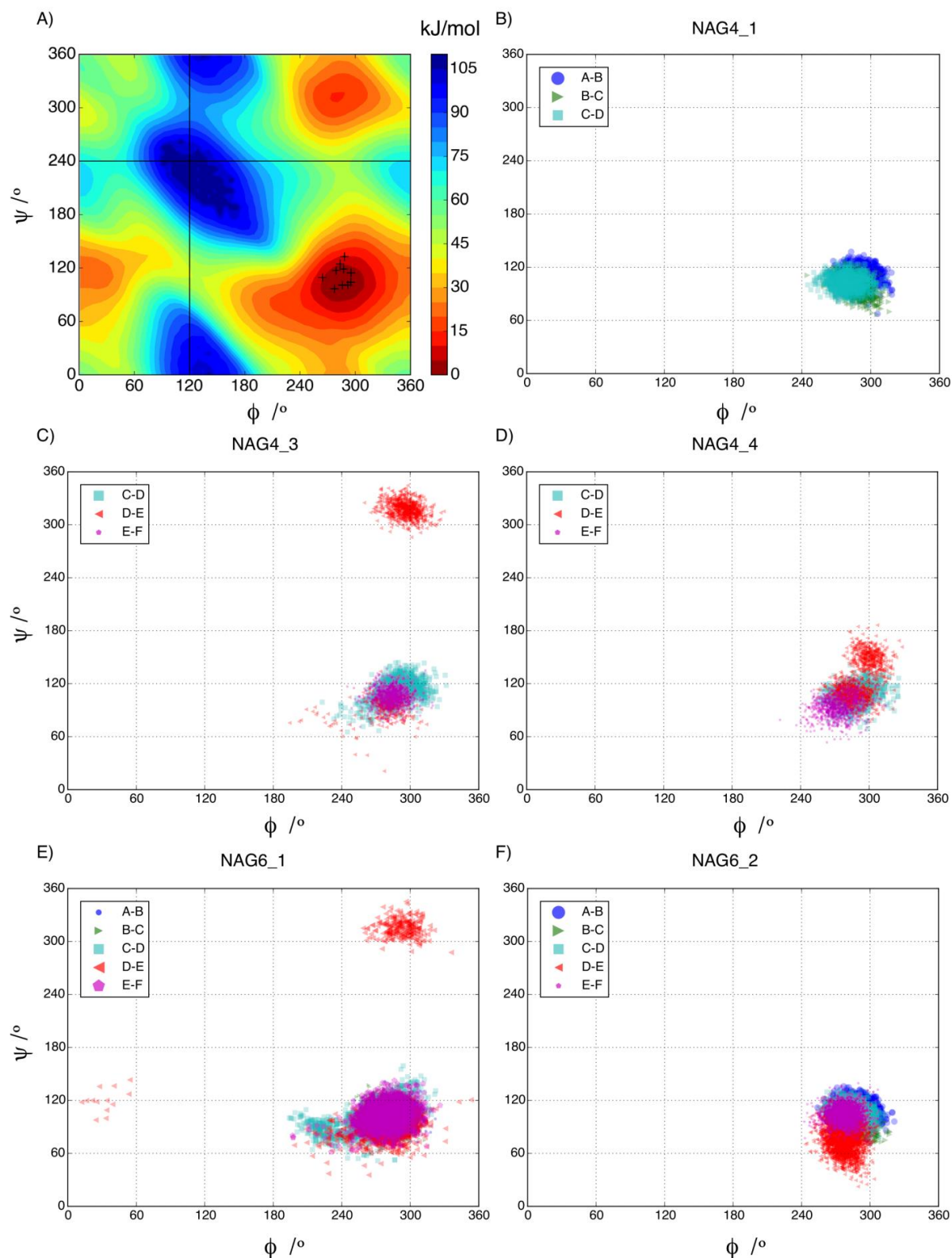


Figure 4. Representation of the glycosidic dihedral angles (ϕ , ψ) of the NAG sugar units populating sites A to F. Panel A shows the free-energy landscape of the β -GlcNAc(1-4)- β -GlcNAc linkage where the red region (0 kJ/mol) shows the lowest free-energy state. Scatter points indicate the glycosidic dihedral angles of the λ lysozyme-NAG6 crystal structure

(PDB ID:3D3D). They all occupy the same region which is the lowest free-energy state for this linkage. The glycosidic dihedral angles of the sugar units (populating sites A to F) observed during the MD simulations are plotted for the NAG4_1 (panel B), NAG4_3 (panel C), NAG4_4 (panel D), NAG6_1 (panel E) and NAG6_2 (panel F) simulations. Only the linkage between the sugars populating the D and E sites (shown in red) adopts a conformation corresponding to the second low free energy state.

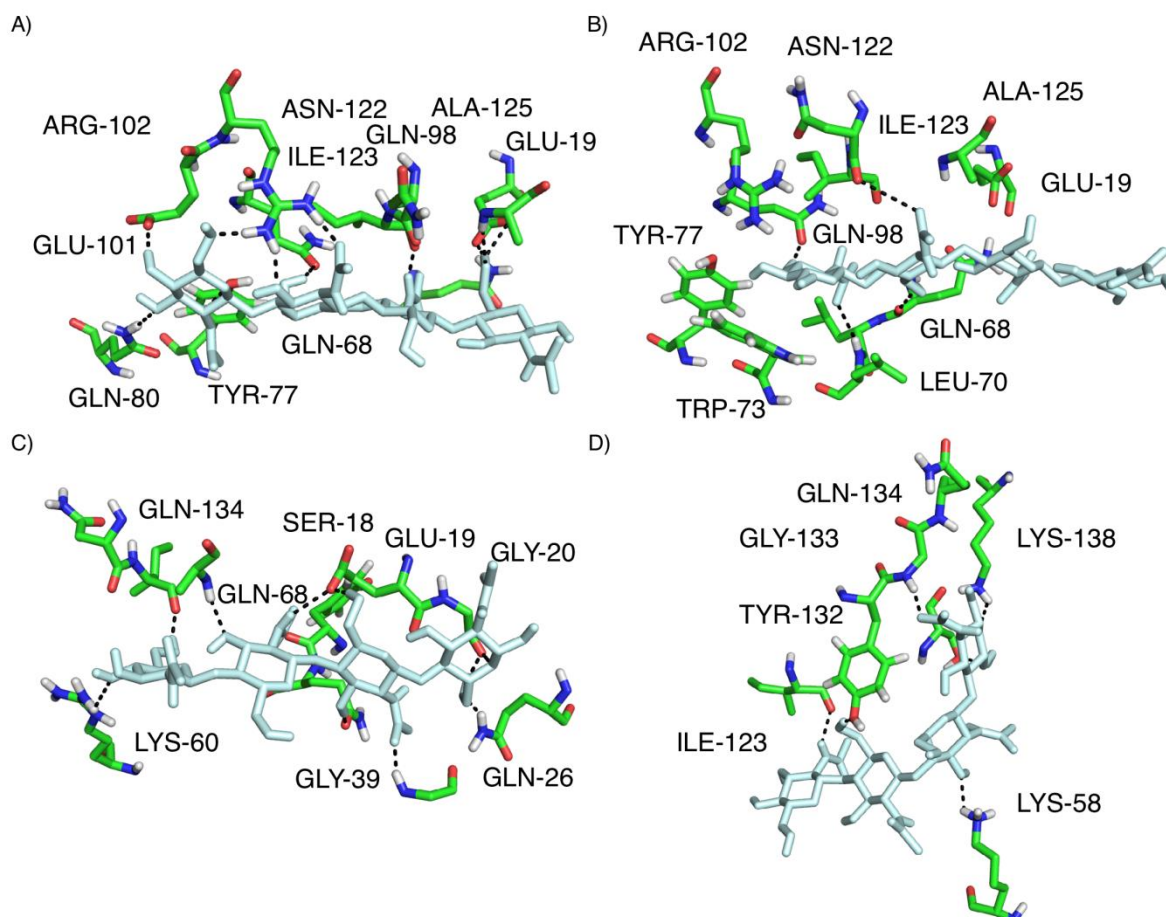


Figure 5. Dynamic hydrogen bonding pattern captured in the MD simulations. Panels show conformations in the λ lysozyme-NAG4 simulations with the key hydrogen bond interactions between sugar (pale cyan) and enzyme (green). The residues involved in these key hydrogen bonds showed significant combined chemical shift changes for their backbone and side chain H^N groups (Table S1). A) and B) show sites ABCD with hydrogen bonding patterns observed in the NAG4_1 simulation. C) shows sites CDEF and D) shows sites CDE^uF^u with hydrogen bonding patterns observed in the NAG4_3 simulation.

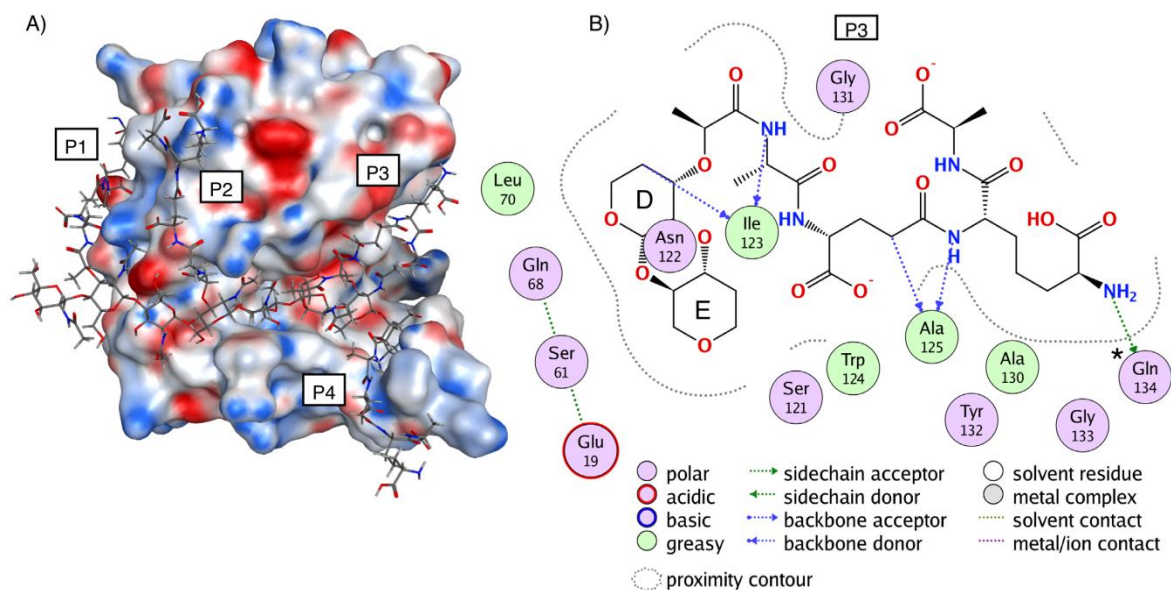


Figure 6. λ lysozyme-peptidoglycan complex. A) λ lysozyme-peptidoglycan complex model represented with the molecular surface of λ lysozyme coloured according to electrostatic potential from the Poisson Boltzmann equation (peptidoglycan is NAG1-NAM1(-P1)-NAG2-NAM2(-P2)-NAG3-NAM3(-P3)-NAG4-NAM4(-P4), where the peptide moieties are labelled P1, P2, P3 and P4). B) Residues of λ lysozyme which interact with the P3 pentapeptide moiety of the peptidoglycan are shown colour-coded according to the nature of the interaction (created with interaction diagram of MOE⁴²). Ile123, Ala125 and Gln134 form hydrogen bonds with the P3 unit. Gln134 also forms strong hydrogen bonding interactions with the sugar in the NAG4_3 and NAG6_1 simulations when significant glycosidic angle changes are observed.